90 nm-thick graphene metamaterial for strong, extremely broadband absorption of unpolarized light

Han Lin[1], Björn C. P. Sturmberg2, Keng-Te Lin[1], Yunyi Yang[1], Xiaorui Zheng[1],Teck K. Chong[3], C. Martijn de Sterke[2*] and Baohua Jia[1*]

[1]*Centre for Micro-Photonics, Faculty of Science, Engineering and Technology, Swinburne University of Technology, P. O. Box 218, Hawthorn VIC 3122, Australia*

[2] *CUDOS and IPOS, School of Physics, University of Sydney, Sydney, 2006, Australia*

[3] *Centre for Sustainable Energy Systems, Research School of Engineering, Australian National University, Canberra 2601, Australia*

E-mail: martijn.desterke@sydney.edu.au, bjia@swin.edu.au

Abstract

Broadband strong light absorption of unpolarized light over a wide range of angles in a large-area ultrathin film is critical for applications like photovoltaics, photodetectors, thermal emitters and optical modulators. Despite long-standing efforts in design and fabrication, it has been challenging to achieve all these desired properties simultaneously. We experimentally demonstrate a 12.5 cm^2, 90 nm-thick graphene metamaterial with approximately 85% absorptivity of unpolarized, visible and near-infrared light covering almost the entire solar spectrum (300-2500 nm). The metamaterial consists of alternating graphene and dielectric layers; a grating couples the light into waveguide modes to achieve broadband absorption over incident angles up to 60°. The very broad spectral and angular responses of the absorber are ideal for solar thermal applications, as we illustrate by showing heating to 160 °C in natural sun light. These devices open a novel approach to applications of strongly absorbing large-area photonic devices based on 2D materials.

The performance of an ideal strong absorber is that of a black body—a material that absorbs radiation at all angles and polarizations, over a broad bandwidth. They have applications in photo thermal energy generation[1-4], desalination[5], thermal emitters[6], modulators[7], detectors[8,9], and concealment[10]. Thick incoherent absorbers, like carbon nanotubes[11,12] or plasmonic nanocomposites[6,13-16] use randomly distributed and oriented nanoparticles to achieve strong absorption. However, their large thickness (10's-100's of micrometers) impedes device integration and can degrade performance[1,6,9]. Thin coherent absorbers have been implemented using plasmonic metamaterials[17-21], dielectric gratings[22] and layered structures composed of 2D materials [23,24], and hyperbolic metamaterial nanoparticles[25]. Though some of these achieve broadband, polarization-independent operation[25], most only achieve single-polarization or narrowband absorption despite their complicated designs,[17,18,26-28] and all require sophisticated nanofabrication. This prevents practical applications that require large areas such as energy harvesting[1] and thermo-photovoltaics[29]. Although omnidirectional, broadband light absorption[30] was recently demonstrated in coated ultrathin metallic film, the suitability of these devices for energy conversion, including photothermal applications, is unproven, because the stability of metallic nanostructures is significantly lower than that of their bulk forms.

Graphene is emerging as a promising candidate for ultrathin strong light absorption due to its outstanding optical properties[31]. The absence of a bandgap in graphene means that it absorbs electromagnetic radiation over a very wide bandwidth, ranging from the ultraviolet to the terahertz regime[31]. Since at visible- and near-infrared frequencies a monolayer of intrinsic graphene has broadband absorption of 2.3%[32], achieving strong absorption requires significant enhancement. A record-high 47.2% absorption in monolayer graphene via a multi-layer structure was demonstrated at $\lambda \approx 13$ μm[23]. Strong light absorption in a single patterned sheet of doped graphene[33,34], and in monolayer graphene sandwiched in a Fabry-Perot cavity structure[35] at $\lambda \approx 1.1$ μm were predicted, as was strong, near-infrared light absorption in a graphene-based hyperbolic metamaterial[24,36]. However, these approaches are limited to a single polarization, and device fabrication remains a challenge. The proposed graphene hyperbolic metamaterial, for example, consisting of alternating graphene and dielectric layers, traditionally requires sophisticated and time-consuming chemical vapour deposition[37]. Therefore, so far there have been no experimental demonstrations of strong light absorption in graphene-based metamaterial.

In this paper, we demonstrate a polarization-independent ultra-broad bandwidth strong light absorption (300-2500 nm) that covers almost the entire solar spectrum over a large angular range, in a graphene-based metamaterial grating of deep subwavelength thickness (90 nm) on a flexible substrate. The metamaterial consists of weakly absorbing alternating graphene layers, separated by lossless dielectric, and it thus fundamentally differs from earlier incoherent and coherent absorbers[1-4]. Unlike other thin-film perfect absorbers[22-24,28,33,34], our device is polarization-independent because a grating couples into TE and TM-polarized guided modes, both of which, by the careful design of the metamaterial, undergo significant absorption. The extraordinary performance of our device is achieved by the seamless combination of different light absorption regimes: at long wavelengths, the presence of the grating is irrelevant and the device acts as a uniform thin film. In the visible part of the spectrum the grating couples light into multiple guided waves and leads to non-specular diffracted orders in the air. At the intermediate near-infrared (NIR) wavelengths the grating excites guided waves but does not lead to non-specular orders in the air.

Our device is fabricated using inexpensive, solution-based layer-by-layer self-assembly (SA), combined with direct laser writing[38]; this enables us to fabricate metamaterial with a large-area (12.5 cm^2), which is limited only by our translation stage. Thus, our cost-effective and scalable graphene absorber is promising for integrated, large-scale applications that require polarization-independent, angle insensitive and broad bandwidth absorption such as energy-harvesting, thermal emitters, optical interconnects, photodetectors and optical modulators. Fabrication on a flexible substrate and the robustness stemming from graphene make it suitable for industrial use[39], and for applications that require conformal coverage, such as concealment[10].

Design of graphene-based metamaterial absorber

The degree of light absorption can be thought of as the product of an interaction length L and an absorption coefficient α, while minimizing reflection. For absorbers based on carbon nanotubes, both α and L are large, and reflection is avoided by a graded surface[11,12]. In comparison, achieving strong light absorption in deep subwavelength thin films is challenging. The interaction length L can be enlarged by coupling the incident light into waves that propagate along the surface, such as surface plasmons or waveguide modes[22,23]. In this way, strong absorption was realized in structures of deep subwavelength thickness[22,23] ,

and which have a grating to effect the coupling. However, the bandwidths was limited to tens of nanometres, and they were strongly polarization-sensitive.

The absorbing element in our structure is a metamaterial consisting of periodically alternating nanometer-thin layers of graphene (thickness t_g) and a dielectric (thickness t_d). Since each of these layers is much thinner than the wavelength of light, the metamaterial behaves like a uniform uniaxial film with effective parameters.[40] The effective in-plane and out-of-plane permittivity are given by the mixing formulae

$$\varepsilon_{\parallel} = f\varepsilon_g + (1-f)\varepsilon_d \tag{1}$$

$$\varepsilon_{\perp} = \left(f\varepsilon_g^{-1} + (1-f)\varepsilon_d^{-1}\right)^{-1} \tag{2}$$

with $f = t_g/(t_g + t_d)$ the graphene filling fraction, ε_d the permittivity of the dielectric, and ε_g the in-plane permittivity of a graphene[37]

$$\varepsilon_g = 1 + \frac{i\sigma}{\varepsilon_0 \omega t_g} \tag{3}$$

where σ is the surface conductivity and ε_0 the vacuum permittivity. ω is the angular frequency. Complete absorption for TE and TM polarizations cannot be achieved since for TM polarization this requires a modest real part since otherwise the field inside the absorber is too weak, whereas the imaginary part needs to be large. In contrast, TE polarization requires a large real part, but a modest imaginary part. By carefully designing our metamaterial through the filling fraction f, we find a compromise where both polarizations are strongly absorbed. We control the thickness of the graphene layers down to nanometer accuracy, while the thickness of the dielectric layer is $t_d = 2$ nm. In this way, the refractive index and extinction coefficient of the metamaterial can be widely tuned (supplementary Fig. S1). High, nearly polarization-independent absorptivity is achieved for $t_g = 1$ nm, for which, according to Fig. S1, the metamaterial's permittivity differs significantly from that of pristine graphene.

The metamaterial film is patterned periodically with one-dimensional air grooves, forming a grating (see Fig. 1). Incident TE-polarized light couples into TE-polarized waveguide modes. The electric field of such modes is parallel to the film, and they are strongly absorbed because a significant fraction of the energy resides in the metamaterial[22]. Incident TM-polarized light couples into TM guided modes, for which the electric field is predominantly perpendicular to the film. Compared to that in air, this field component is reduced by a factor

$\varepsilon_\perp$ (Eq. 2) in the metamaterial; TM modes therefore have less energy in the metamaterial, lowering the absorptivity[22]. To ensure that the absorptivity is polarization-independent, compared to the previous work[22] the metamaterial needs to have: high intrinsic absorptivity; larger thickness; and lower permittivity. Our graphene-based metamaterial allows us to achieve all of these requirements simultaneously: even though the metamaterial contains dielectric, it nonetheless absorbs strongly; our fabrication technique allows us to fabricate 90 nm thick metamaterial; and the permittivity of the metamaterial can be lowered through the relative thicknesses of the dielectric and the graphene layers (supplementary Fig. S1). The combination of the grating metamaterial with a silver mirror and a SiO_2 spacer layer (see Fig. 1) ensures that reflected light striking the absorber from below does not interfere destructively with the incident light.

As the graphene material has already demonstrated high absorptivity at visible wavelengths[32], we initially design the absorber so as to increase the absorptivity in the near infrared wavelength region of 800-1200 nm. A set of numerical simulations of the structure was carried out using the EMU stack package[41,42]. The metamaterial has a thickness d = 90 nm, and the effect of laser photoreduction is included by modifying the graphene oxide properties (see Methods). The grating period is p = 980 nm and the width of the air grooves is g = 500 nm. Thus in the range 980-1200 nm and at normal incidence, there are no propagating non-specular diffraction orders in the air. The SiO_2 spacer layer has a permittivity $\varepsilon_d = 2.25$, and a thickness h_s = 80 nm. The silver mirror is 100 nm thick. The calculated absorptivity versus wavelength and incident angle for TE and TM polarized light, as well as for unpolarized light, are shown in Figs. 2a, b and c, respectively. Figures 2d, e, and f show the absorptivity versus wavelength when averaged over 0°-20° (solid lines) and 0°-40° (dashed lines) incident angles. TE-polarized light is calculated to have nearly flat absorptivity of up to 94% over an almost 300 nm spectral range (Figs. 2a,d), while for TM polarization the absorptivity exceeds 80% (Figs. 2b,e). The absorptivity of unpolarized light exceeds 80% over the entire bandwidth examined (Figs. 2c, f). The absorption in the silver layer is $\lesssim$0.5% for unpolarized light. Even though for λ<980 nm the grating leads to propagating, non-specular orders in the air, which act as additional channels for the light to exit the absorber, this does not seem to affect the absorptivity.

Fabrication of the absorber

The fabrication of the metamaterial consists of three steps (Fig. 3a): 1) Deposition of the silver mirror and the SiO_2 spacer on a substrate; 2) Self-assembly of the GO and dielectric multilayers; 3) Reduction of the GO, and fabrication of the grating by femtosecond laser writing.

The silver mirror and SiO_2 spacer layer are deposited by physical vapour deposition. The graphene based metamaterial layer is fabricated by using the wet chemical Self-Assembly (SA) technique (see supplementary section S2), in which negatively charged GO layers and positively charged Polydiallyldimethylammonium chloride (PDDA) are alternately deposited thanks to a static electric force[43] (supplementary section S2). The thickness of the dielectric layer is controlled by the choice of the dielectric material, while the thickness of a GO layer is controlled by the concentration of the GO solution and the layer thickness of the GO flakes in the solution, which is 1~2 layers (supplementary section S2). GO is a graphene network with oxygen containing groups. An AFM is used to measure the thickness of each layer and the surface roughness. A layer thickness of 2 nm of the GO layer can be accurately achieved, while the surface roughness, which plays a key role in photonic applications, can be controlled to less than 2 nm on average.

The grating was fabricated using a tightly focused femtosecond laser beam[38]. We used λ=800 nm, 100 fs laser pulses, which were focused by a 0.8 numerical aperture (NA) objective lens. The beam also reduces some of the GO (Fig. 3a)[44,45]. The removal of oxygen containing groups and the recovery of the sp2 graphene network is demonstrated by X-ray photoelectron spectroscopy (XPS) spectra (supplementary Figs. S6 and S7). Because the photo-reduction is based on the photo-thermal effect (supplementary section S3), the extent of the reduction can be finely tuned by the laser power. With high enough power (around 60 μW in this study), the GO layers are converted to graphene-like material in which the oxygen containing groups are near completely removed[38] (supplementary section S3). In this process 2 nm thick GO layers are converted to approximately 1 nm thick graphene layers, because the atomic layer spacing is reduced from 8.1 Å of GO to 3.4 Å of graphene[38].

An optical photograph of our 25 × 50 mm^2 (supplementary Fig. S11) graphene absorber is shown in Fig. 3b, which was taken with a 633 nm long-pass filter. The dark regions indicate the grating. Gratings with different orientations, indicated by the bar patterns, look very similar, consistent with polarization-independent performance. The curved surface allows us to see the strong absorption of light incident at different angles. Fig. 3c shows a reflection

optical microscope image of the grating; it is well-defined thanks to the high uniformity of the metamaterial and the precise laser writing control. The SEM image in Fig. 3d shows that a linewidth down to 400 nm can be achieved. The smoothness is confirmed by a large-area measurement using an optical profiler (Fig. 3e). The cross section in Fig. 3f confirms that the grooves are smooth and have a full width at half maximum (FWHM) of 500 nm, limited by the resolution of the optical profiler.

One of the advantages of graphene is its tunable optical bandgap. While usually controlled by doping,[37] here we use laser reduction[38,46], allowing us to pattern the samples without high vacuum processing. Fig. S10a (dashed curves) shows the effective permittivity of the GO multilayer, measured by spectral ellipsometry. Both the real and imaginary parts have weak wavelength dependence between 800 nm to 1150 nm. The real and imaginary parts of the effective permittivity of the graphene film (solid curves), have increased significantly due to the formation of graphene after photo-reduction, which increases the conductivity σ, consistent with Eq. (3). The polymer layers lower the effective permittivity of the metamaterial compared to pure laser converted graphene film made using the filtration method[38] or that of pristine graphene[47].

Experimental results

The reflection (R) from the graphene-based absorber was measured and the absorptivity (A) was determined through $A = 1 - R$, since the Ag bottom reflector prevents light transmission. In our first experiments, we characterized the reflectance of 60×60 μm^2 samples using a Fourier transform infrared (FTIR) spectrometer (Bruker Hyperion 2000) with an optical microscope setup. We studied the angular absorption with a 15× 0.4 NA, wide-angle reflection microscope objective (see the inset of Fig. 4a). The specular reflection was measured over an optical cone ranging from θ_1=12° to θ_2=23.6°. A near-infrared polarizer (wavelength range 0.8-5.0 μm) controlled the polarization of the incident light. Fig. 4a shows the measured absorptivity for TE polarization, TM polarization and for unpolarized light, which was taken to be the average. The measured absorptivity of the metamaterial without a grating was approximately 10% for unpolarized light, confirming that the grating is essential to achieve high absorptivity.

Fig. 4a shows that for TE polarization absorptivity can be up to 95%, and is almost constant over the entire spectral range of more than 300 nm. The absorptivity of TM polarized light is as high as 80% and exceeds 70% over this bandwidth. As a result, the absorptivity of

unpolarized light reaches 90%, and easily exceeds 80% over the entire spectral range. To confirm the weak angular dependence further, we used microscope objectives with different convergence angles, resulting in absorptivity of over 85% in all cases (supplementary Figs. S12 and S13), consistent with simulation (supplementary Fig. S14).

The flexibility of the laser writing allows us to tune the width of the ablated lines, and thus the duty cycle (defined as $(p\text{-}g)/p$ in Fig. 1) of the grating, providing control of the absorptivity. An increase of laser power leads to an increased width of the ablated area, and thus to a lower duty cycle. Tuning the laser power from 70 μW to 140 μW leads to duty cycles from 0.8 to 0.25. We fabricated 16 samples with similar performance (supplementary Fig. S15) using different laser powers. Fig. 4b show that high absorptivity (>70%) of unpolarized light can be achieved for this entire range, confirming the robustness of our approach. The absorptivity is largest for laser powers of 100 μW (Fig. 4c) with 40% duty cycle, consistent with simulations.

Based on the optimized processing parameters, we fabricated a large-area graphene-based metamaterial absorber (25 × 50 mm^2, Fig. 3b) and tested its photothermal performance. The absolute absorptivity covering the solar spectrum was measured by UV-VIS-NIR spectrometer (Perkin Elmer-Lambda 1050, with an integration sphere). We measured the absorptivity of GO metamaterial and of reduced metamaterial with the same configuration, as references. As shown in Fig.5a, the absorptivity of the metamaterial device is approximately 85% over the entire 300-2500 nm wavelength range, which covers almost the entire solar spectrum. This means that our device absorbs more than 86% of the incoming solar energy flux. As expected, the GO metamaterial has low absorptivity (10%) over the entire spectrum, though it increases significantly upon reduction, especially in the visible. The grating further enhances the absorptivity in the NIR region, resulting in large-bandwidth, high absorption, that ranges from 83% to 88%. Fig. 5b shows that our device absorbs not only over a broad bandwidth, but also over a large range of incident angles.

With a period of $d = 980$ nm, and metamaterial refractive index of $n \approx 2.5$, the grating excites guided modes in the metamaterial over almost the entire wavelength range at normal incidence. At the longest wavelengths the metamaterial acts as a highly efficient uniform absorber, even though the conditions for perfect absorption are not satisfied[22,48]. While for shorter wavelengths the gratings excites guided modes in the metamaterial, for λ>980 nm only the reflected specular order can carry energy away from the absorber. For λ<980 nm,

there are multiple diffracted orders in the air. Our simulations show that the energy carried away by these orders is less than 15%, and is likely to be lower due to the variations in the grating parameters. The combination of the broadband absorption of graphene, the enhanced interaction between the grating and the metamaterial through the excitation of guided modes, and the limited scope for light reflection, produce the measured absorptivity above 80% throughout the measured wavelength range. Thus while the absorption mechanism at each wavelength is known, our device achieves its extraordinary broad bandwidth by the seamless combination of these mechanisms as the wavelength is varied.

We used an IR camera (Testo 890-2 Professional TI) to study the photo-thermal performance of the absorber under natural sunlight in an open environment (Fig. 5c), resulting in the photo-thermal image in Fig. 5d. Fig. 5e shows temperature versus time for GO metamaterial (red), for which the temperature increase is approximately 10 °C, and for our sample (blue) for which the temperature increases by 130 °C with a characteristic time of approximately 10 s. Therefore, the graphene-based metamaterial absorber exhibits outstanding photothermal characteristics. For thick hierarchical graphene foam absorber[3], shown for comparison, the temperature increases by approximately 20 °C (green). The high absorptivity in our devices, combined with the small volume is ideal for efficient energy extraction in photo-thermal applications. Heat generated in thick absorbers[2-4] is difficult to extract because it is stored in the entire volume, while, typically, heat can only be extracted from the surface. Heat extraction by circulating water inside the absorber adds complexity[14]. Defining the Figure of Merit (FoM) $\Delta\lambda/\lambda_p$, where λ_p is the peak absorptivity wavelength and $\Delta\lambda$ is its FWHM, we compare our results and fabrication characteristics with the state-of-the-art, optical thin absorbers (supplementary table S4). Our absorber has the largest bandwidth among all optically thin absorbers, combined with a higher absorptivity and suitability for large-scale fabrication.

Conclusions

In conclusion, we report a graphene-based metamaterial absorber, deposited on a dielectric spacer layer and backed by a mirror, with a grating that is fabricated using a tightly focused femtosecond laser. The absorber has broad-bandwidth absorption of well over 80% of unpolarized light over almost the entire solar spectrum (300-2500 nm), which makes it suitable for high-performance solar thermal applications. The low dispersion of graphene is central to achieving the ultra-broadband absorption, therefore, the absorber can, in principle,

be scaled to other wavelength ranges. Since the intrinsic absorptivity of single graphene layers is low, the high absorption requires relatively large number of graphene layers. However, direct stacking of graphene layers results in graphite, which has different optical properties. The use of the metamaterial, in which the graphene layers are separated by polymer, allows us to stack the graphene while maintaining their optical properties, thus leading to strong, broadband absorption. Incorporating graphene in a metamaterial also lowers the effective permittivity so as to achieve absorption of both TE and TM polarizations.

The metamaterial is fabricated using a scalable, high-yield, robust, low-cost, solution-based, layer-by-layer SA method. While our lasers limit our samples to an area of approximately $50\times25\ \mathrm{mm}^2$, samples as large as a square meter can be fabricated using industrial-scale facilities[49]. Since the optical properties of our metamaterials can be dialled-in by varying the graphene to polymer ratio, and can even be non-uniform, our fabrication technology opens new avenues for applying 2D materials to enable novel and functional optoelectronic devices.

Methods:

Graphene metamaterial fabrication and characterization

The aqueous GO dispersion was synthesized by chemical oxidization of graphite via the modified Hummers Method[50]. Then homogenous graphene metamaterial with controllable thicknesses were prepared using self-assembly (see Supplementary section S2). The large area graphene was produced by photo-reduction of GO using a femtosecond laser (Libra, 800 nm, 100 fs, 10 kHz). Elemental chemical composition was characterized using X-ray photoelectron spectroscopy (XPS, ESCALAB 250). The thickness and the optical properties of the GO and graphene metamaterial were characterized by an AFM and an ellipsometer (M-2000 J.A. Woollam Co), respectively.

Laser fabrication of nanogratings

A femtosecond laser beam (Libra, 100 fs pulse, 10 kHz repetition rate, 800 nm wavelength) going through the dichroic mirror was focused by a high numerical aperture (NA) objective lens (100×, NA=0.85) onto the GO sample, which was mounted on a 3D nanometric piezo-electric stage (PhysikInstrumente®). A computer-controlled system was used to control the parameters of the laser photo-reduction process, including laser power, scanning speed and patterns. The ablation threshold power was found to be 70 μW, corresponding to a pulse

energy of 7 nJ. The air grooves start to overlap when the power is higher than 140 μW (14 nJ pulse energy). These two powers define the lower and upper limits of the laser power range, which is explored in 10 μW steps. Since the laser focal spot has a full width at half maximum (FWHM) of 600 nm, the laser energy density in the centre of the focal spot varies between 2.8 J/cm^2 to 5.6 J/cm^2. The scanning speed was 100 μm/s to ensure smooth line fabrication.

FTIR measurement of reflectance

At infrared wavelengths from 400 cm^{-1} to 12500 cm^{-1}, a Fourier transform infrared (FTIR) spectrometer (Bruker Hyperion 2000) was used to characterize the reflectance of the samples, with a cover glass coated with 100 nm-thick silver film used as a reference. The sampling step in wave number is 8 cm^{-1}. A silicon photo-detector was used to acquire the signal.

UV-VIS measurement of broadband absorption

A UV-VIS spectrometer with an integration sphere (Perkin Elmer-Lambda 1050) was used to characterize the absorptivity of the large area sample in the wavelength range 300-2500 nm, using air as a reference. The wavelength sampling step is 10 nm.

Thermal imaging and temperature measurement

The thermal images were taken by an IR camera (Testo 890-2 Professional TI with 640x480 Detector), and the temperature was determined using Testo IRsoft software.

Numerical simulation

The comprehensive theoretical study of the phenomenon was carried out using the EMUstack package[41,42] for numerical simulations. We first performed a characterization study in which we numerically calculated the TE and TM absorptivity spectra for a wide range of design parameters: graphene filling fraction, grating period, grating duty cycle, grating thickness, and spacer layer thickness. EMUstack is ideally suited to such a parameter survey because it uses a highly efficient one-dimensional solver and handles variations in layer thicknesses analytically thereby requiring negligible additional computation time to calculate many thicknesses simultaneously[42]. Once these parameters were determined, these were combined with other parameters, which we could measure directly.

After numerically confirming that the fine structure of the graphene and polymer dielectric layers does not matter for the optical properties, we ignored this fine structure, instead using the effective permittivity of the reduced metamaterial (shown in Fig. 3f) as this quantity can

be directly measured. The fabricated samples have significant variation in the thickness of the rulings (see Fig. 3e), which was not included in the numerical calculations and which leads to the fabricated samples having improved broadband absorptivity compared to the numerical simulations.

In each simulation we include 25 angles within the angular cone of $\pm(12° - 24°)$, matching the objective used for the characterization, and we then averaged over these spectra.

Data Availability Statement

The data that support the plots within this paper and other findings of this study are available from the corresponding authors upon reasonable request.

Author contributions

H.L., B.S., C.M.de S., and B.J. conceived original idea and proposed the project. H.L. X.Z. and Y.Y. carried out experiments including GO film synthesis, laser fabrication and characterizations. B.S. and C.M. de S. developed the theoretical models and numerical simulations. T.C. coated Ag reflector and SiO_2 spacer layer on silicon substrates. H.L. and K.L. performed the thermal imaging and temperature measurement. H.L., K.L., B.S., C.M de S. and B.J. contributed to data analysis and writing and revising the manuscript. C.M de S. and B. J. supervised the project. All authors discussed the results and commented on the manuscript.

Figure captions

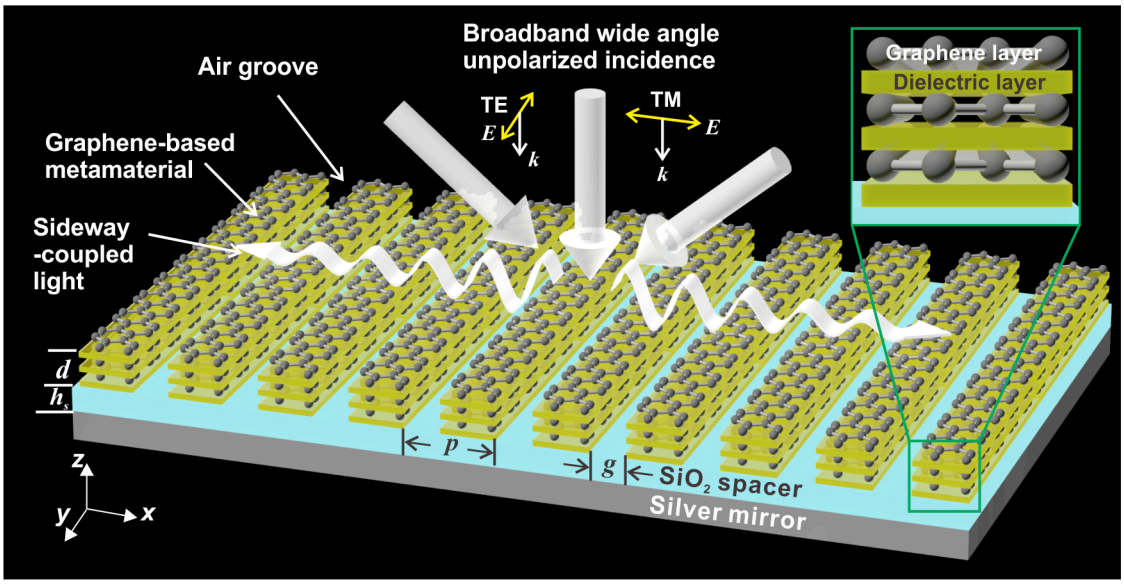

Fig. 1. Schematic of graphene-based metamaterial absorber. Broadband, unpolarized light is incident from a wide range of incident angles. The grating couples the light side-ways into waveguide modes that propagate along the surface, leading to large absorption in the metamaterial. Inset shows the structure of the metamaterial.

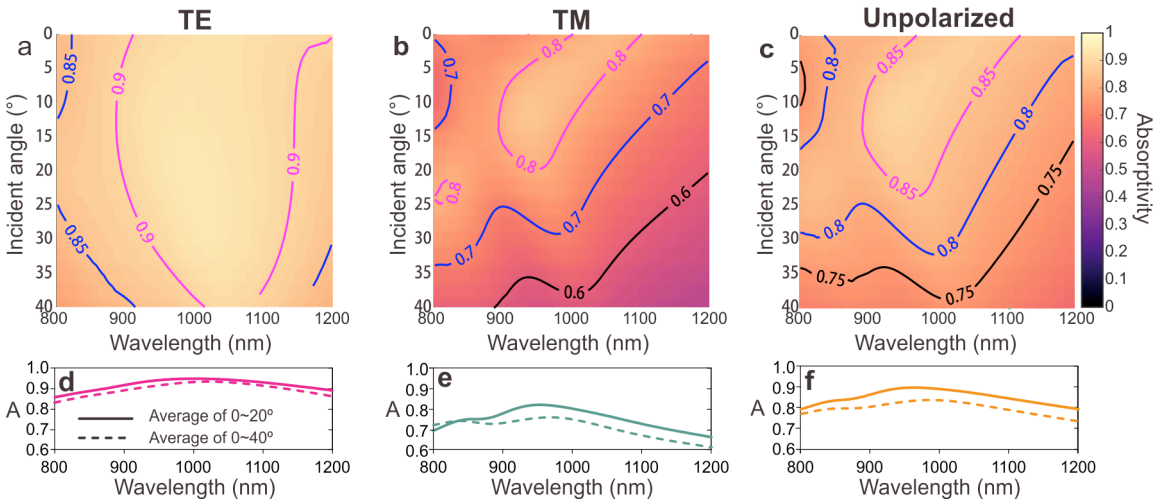

Fig. 2. Calculated absorptivity spectra of graphene-based material absorber. Calculated absorptivity versus wavelength and angle of incidence for (a) TE, (b) TM, and (c) unpolarized light. Absorptivity averaged over incident angles from 0° to 20° (solid curves) and 0° to 40° (dashed curves) of (d) TE, (e) TM, and (f) unpolarized light.

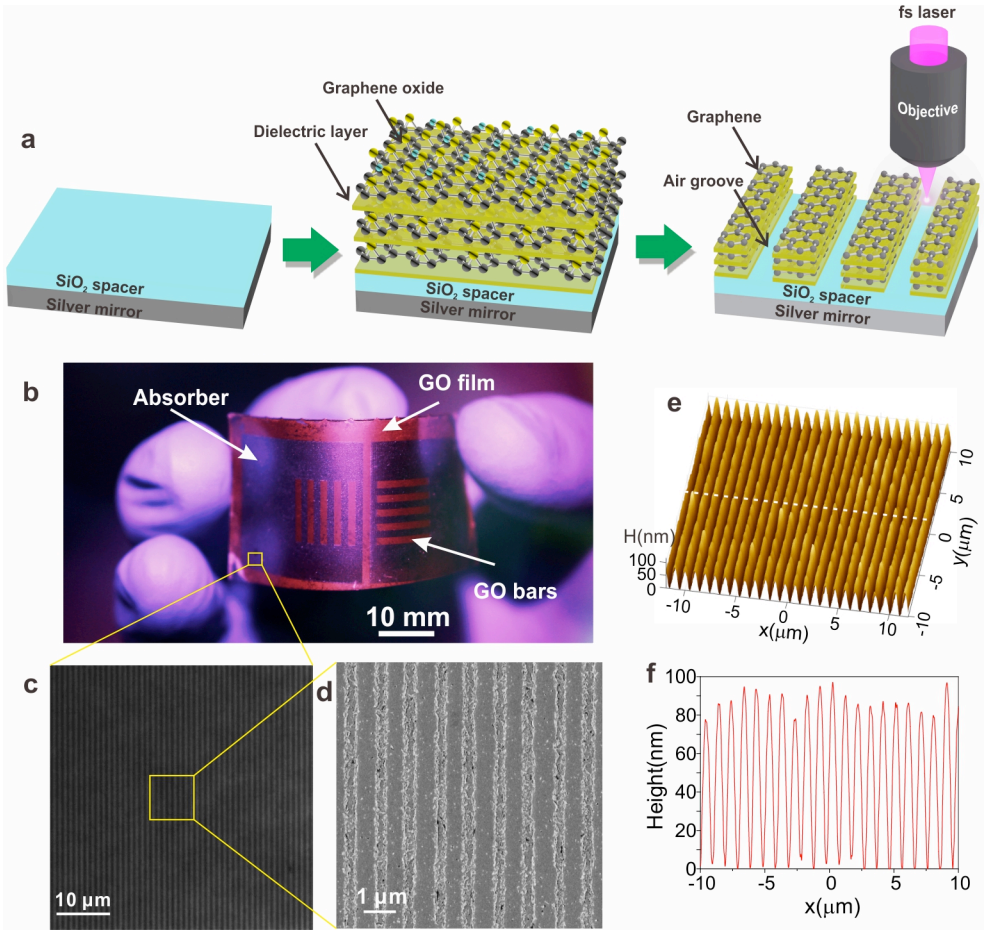

Fig. 3. Fabrication process and results of graphene-based metamaterial absorber. (a) Schematic of the fabrication of our graphene-based metamaterial absorber; (b) Photograph of the absorber with an area of 50 mm by 25 mm through a 633 nm long pass filter. The dark area indicates our absorber; (c) Optical microscopic image of the grating; (d) SEM image of the central part of the grating; (e) optical profiler image of the grating; (f) Cross-section of the optical profiler image.

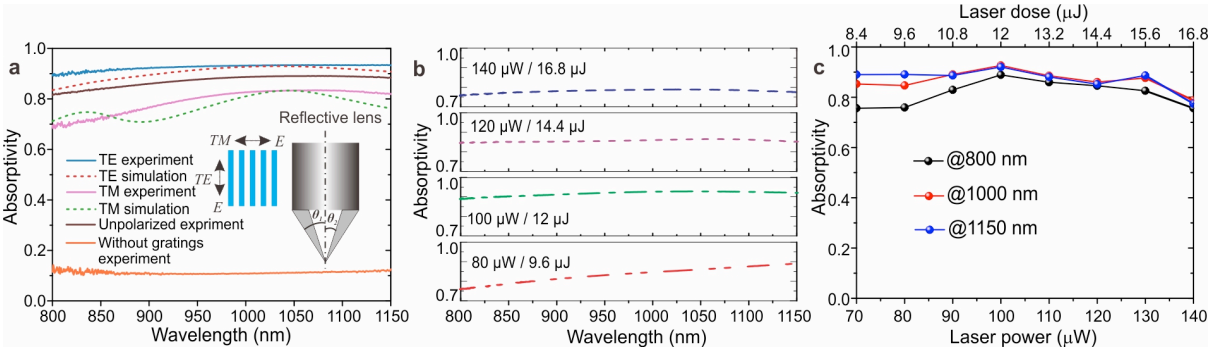

Fig. 4. Measured absorptivity spectra of graphene-based metamaterial absorber (a) Measured absorptivity spectra (solid curves) for TE and TM polarization and for unpolarized light. Shown for comparison are the metamaterial absorptivity without a grating (orange solid curve) and the calculated absorptivity spectra (dashed curves). Inset, schematic of the definition of TM and TE polarization, and the light cone of the reflective objective lens used for the FTIR measurement. (b) Measured absorptivity spectra of unpolarized light from gratings fabricated with laser powers (doses) of 80 μW (9.6 μJ), 100 μW (12 μJ), 120 μW (14.4 μJ) and 140 μW (16.8 μJ), respectively. (c) Absorptivity versus laser power and laser dose at three wavelengths.

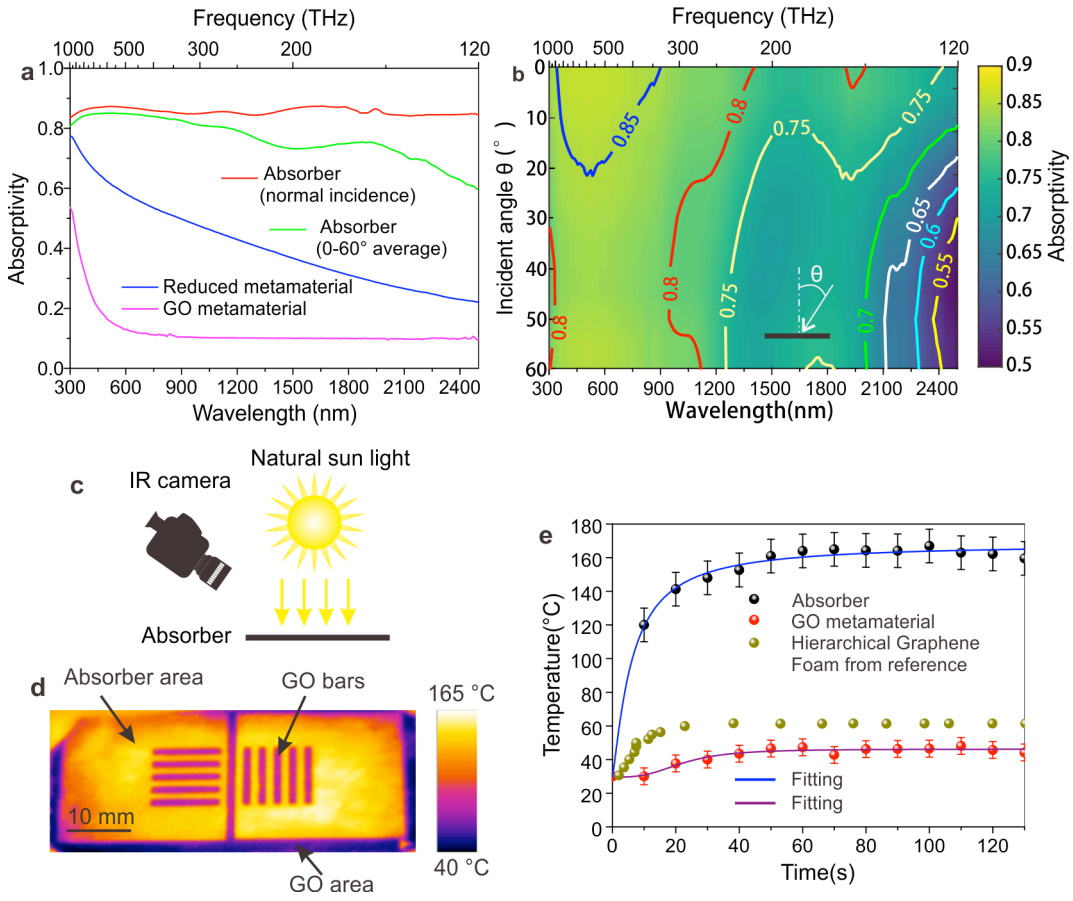

Fig. 5 Measured absorptivity spectra and photo-thermal performance of a large-area graphene-based metamaterial absorber (a) Absorptivity spectra at the normal incidence of our graphene metamaterial absorber (red), absorber with angle averaged absorptivity from 0 to 60° (green), GO (magenta) and reduced GO (blue) metamaterials. (b) Absorptivity versus wavelength and incident angle for our graphene metamaterial absorber measured by an integrating sphere. (c) Schematic of the setup to measure the heating of the sample under sunlight. (d) Thermal image of the fabricated large-area absorber sample. (d) Temperature measurement of the GO metamaterial (red), the graphene-based metamaterial absorber (black) and hierarchical graphene foam (green).[3]

Reference

1 Cao, A., Zhang, X., Xu, C., Wei, B. & Wu, D. Tandem structure of aligned carbon nanotubes on Au and its solar thermal absorption. *Solar energy materials and solar cells* **70**, 481-486 (2002).

2 Ghasemi, H. *et al.* Solar steam generation by heat localization. *Nature communications* **5**, ncomms5449 (2014).

3 Ren, H. *et al.* Hierarchical Graphene Foam for Efficient Omnidirectional Solar–Thermal Energy Conversion. *Advanced Materials* **29** (2017).

4 Zhu, M. *et al.* Tree□Inspired Design for High□Efficiency Water Extraction. *Advanced Materials* (2017).

5 Li, X. *et al.* Graphene oxide-based efficient and scalable solar desalination under one sun with a confined 2D water path. *Proceedings of the National Academy of Sciences* **113**, 13953-13958 (2016).

6 Huang, J. *et al.* Harnessing structural darkness in the visible and infrared wavelengths for a new source of light. *Nature nanotechnology* **11**, 60-66 (2015).

7 Yao, Y. *et al.* Electrically tunable metasurface perfect absorbers for ultrathin mid-infrared optical modulators. *Nano letters* **14**, 6526-6532 (2014).

8 Li, W. & Valentine, J. Metamaterial perfect absorber based hot electron photodetection. *Nano letters* **14**, 3510-3514 (2014).

9 Mellouki, I., Bennaji, N. & Yacoubi, N. IR characterization of graphite black-coating for cryogenic detectors. *Infrared physics & technology* **50**, 58-62 (2007).

10 Shi, H., Ok, J. G., Won Baac, H. & Jay Guo, L. Low density carbon nanotube forest as an index-matched and near perfect absorption coating. *Applied Physics Letters* **99**, 211103 (2011).

11 Mizuno, K. *et al.* A black body absorber from vertically aligned single-walled carbon nanotubes. *Proceedings of the National Academy of Sciences* **106**, 6044-6047 (2009).

12 Xu, T. *et al.* Structural colors: from plasmonic to carbon nanostructures. *Small* **7**, 3128-3136 (2011).

13 Hedayati, M. K., Faupel, F. & Elbahri, M. Tunable broadband plasmonic perfect absorber at visible frequency. *Applied Physics A* **109**, 769-773 (2012).

14 Zhou, L. *et al.* 3D self-assembly of aluminium nanoparticles for plasmon-enhanced solar desalination. *Nature Photonics* **10**, 393-398 (2016).

15 Zhou, L. *et al.* Self-assembled spectrum selective plasmonic absorbers with tunable bandwidth for solar energy conversion. *Nano Energy* **32**, 195-200 (2017).

16 Hedayati, M. K. *et al.* Design of a perfect black absorber at visible frequencies using plasmonic metamaterials. *Advanced Materials* **23**, 5410-5414 (2011).

17 Aydin, K., Ferry, V. E., Briggs, R. M. & Atwater, H. A. Broadband polarization-independent resonant light absorption using ultrathin plasmonic super absorbers. *Nature communications* **2**, 517 (2011).

18 Landy, N., Sajuyigbe, S., Mock, J., Smith, D. & Padilla, W. Perfect metamaterial absorber. *Physical review letters* **100**, 207402 (2008).

19 Massiot, I. *et al.* Metal nanogrid for broadband multiresonant light-harvesting in ultrathin GaAs layers. *ACS Photonics* **1**, 878-884 (2014).

20 Ding, F. *et al.* Ultrabroadband strong light absorption based on thin multilayered metamaterials. *Laser & Photonics Reviews* **8**, 946-953 (2014).

21 Wu, D. *et al.* Numerical Study of the Wide□angle Polarization□Independent Ultra□Broadband Efficient Selective Solar Absorber in the Entire Solar Spectrum. *Solar RRL* **1** (2017).

22 Sturmberg, B. C. *et al.* Total absorption of visible light in ultrathin weakly absorbing semiconductor gratings. *Optica* **3**, 556-562 (2016).
23 Zhu, L. *et al.* Angle-selective perfect absorption with two-dimensional materials. *Light: Science & Applications* **5**, e16052 (2016).
24 Xiang, Y. *et al.* Critical coupling with graphene-based hyperbolic metamaterials. *Scientific reports* **4**, 5483 (2014).
25 Riley, C. T. *et al.* Near-perfect broadband absorption from hyperbolic metamaterial nanoparticles. *Proceedings of the National Academy of Sciences* **114**, 1264-1268 (2017).
26 Luo, H., Cheng, Y. & Gong, R. Numerical study of metamaterial absorber and extending absorbance bandwidth based on multi-square patches. *The European Physical Journal B* **81**, 387-392 (2011).
27 Popov, E. *et al.* Total absorption of unpolarized light by crossed gratings. *Optics express* **16**, 6146-6155 (2008).
28 Lee, K.-T., Ji, C. & Guo, L. J. Wide-angle, polarization-independent ultrathin broadband visible absorbers. *Applied Physics Letters* **108**, 031107 (2016).
29 Lin, S.-Y., Moreno, J. & Fleming, J. Three-dimensional photonic-crystal emitter for thermal photovoltaic power generation. *Applied Physics Letters* **83**, 380-382 (2003).
30 Li, Z., Palacios, E., Butun, S., Kocer, H. & Aydin, K. Omnidirectional, broadband light absorption using large-area, ultrathin lossy metallic film coatings. *Scientific reports* **5** (2015).
31 Koppens, F. *et al.* Photodetectors based on graphene, other two-dimensional materials and hybrid systems. *Nature nanotechnology* **9**, 780-793 (2014).
32 Nair, R. R. *et al.* Fine structure constant defines visual transparency of graphene. *Science* **320**, 1308-1308 (2008).
33 Ferreira, A. & Peres, N. Complete light absorption in graphene-metamaterial corrugated structures. *Physical Review B* **86**, 205401 (2012).
34 Thongrattanasiri, S., Koppens, F. H. & de Abajo, F. J. G. Complete optical absorption in periodically patterned graphene. *Physical review letters* **108**, 047401 (2012).
35 Ferreira, A., Peres, N., Ribeiro, R. & Stauber, T. Graphene-based photodetector with two cavities. *Physical Review B* **85**, 115438 (2012).
36 Nefedov, I. S., Valaginnopoulos, C. A. & Melnikov, L. A. Perfect absorption in graphene multilayers. *Journal of Optics* **15**, 114003 (2013).
37 Chang, Y.-C. *et al.* Realization of mid-infrared graphene hyperbolic metamaterials. *Nature communications* **7**, 10568 (2016).
38 Zheng, X. *et al.* Highly efficient and ultra-broadband graphene oxide ultrathin lenses with three-dimensional subwavelength focusing. *Nature communications* **6**, 8433 (2015).
39 Kaltenbrunner, M. *et al.* Ultrathin and lightweight organic solar cells with high flexibility. *Nature communications* **3**, 770 (2012).
40 Fang, A., Koschny, T. & Soukoulis, C. M. Optical anisotropic metamaterials: Negative refraction and focusing. *Physical Review B* **79**, 245127 (2009).
41 Dossou, K. B. *et al.* Modal formulation for diffraction by absorbing photonic crystal slabs. *JOSA A* **29**, 817-831 (2012).
42 Sturmberg, B. C. *et al.* EMUstack: an open source route to insightful electromagnetic computation via the Bloch mode scattering matrix method. *Computer Physics Communications* **202**, 276-286 (2016).
43 Kotov, N. A., Dékány, I. & Fendler, J. H. Ultrathin graphite oxide–polyelectrolyte composites prepared by self□assembly: Transition between conductive and non□conductive states. *Advanced Materials* **8**, 637-641 (1996).

44 Zhang, Y. L. *et al.* Photoreduction of graphene oxides: methods, properties, and applications. *Advanced Optical Materials* **2**, 10-28 (2014).
45 Zheng, X., Jia, B., Chen, X. & Gu, M. In Situ Third□Order Non□linear Responses During Laser Reduction of Graphene Oxide Thin Films Towards On□Chip Non□ linear Photonic Devices. *Advanced Materials* **26**, 2699-2703 (2014).
46 Guo, L. *et al.* Laser□Mediated Programmable N Doping and Simultaneous Reduction of Graphene Oxides. *Advanced Optical Materials* **2**, 120-125 (2014).
47 Kravets, V. *et al.* Spectroscopic ellipsometry of graphene and an exciton-shifted van Hove peak in absorption. *Physical Review B* **81**, 155413 (2010).
48 Petit, R. & Bouchitté, G. in *Scattering and Diffraction.* 54-62 (International Society for Optics and Photonics).
49 Booth, H. Laser processing in industrial solar module manufacturing. *J. Laser Micro/Nanoeng* **5**, 183-191 (2010).
50 Hummers Jr, W. S. & Offeman, R. E. Preparation of graphitic oxide. *Journal of the American Chemical Society* **80**, 1339-1339 (1958).

Acknowledgement

B.J. and K.L. acknowledge the support from the Australian Research Council (DP190103186). Discussions with Kylie Catchpole and Tom White from the Australian National University during the early stages of this research are gratefully acknowledged.

Materials & Correspondence

Correspondence and requests for materials should be addressed to C.M.de S., and B.J.

Competing financial interests

The authors declare no competing financial interests.